Precision measurement of the Stark shift of the cesium D lines

L. R. Hunter, D. Krause, Jr., S. Murthy, and T. W. Sung
Department of Physics, Amherst College, Amherst, Massachusetts 01002
(Received 10 August 1987; revised manuscript received 30 November 1987)

The dc Stark shift of the cesium D lines is observed in the low-field limit where the induced shift is small compared with the various hyperfine splittings. On the $D2$ line, modification by the electric field of the dipole transition rates to the various excited-state hyperfine levels must be taken into account in order to interpret our results. From our observations the following atomic polarizabilities in units of 10^{-24} cm^3 are deduced: $\alpha_0(6P_{1/2})-\alpha_0(6S_{1/2})=143.8\pm1.4$, $\alpha_0(6p_{3/2})-\alpha_0(6S_{1/2})=187.3\pm1.9$, and $\alpha_2(6P_{3/2})=-38.6\pm1.2$.

I. INTRODUCTION

We are presently pursuing a search for a permanent electric dipole moment (EDM) of Cs in our laboratory. In order to have confidence in this measurement, a thorough understanding of the Stark shift of the $D1$ and $D2$ lines of Cs is required. With the recent success of parity-violation experiments in Cs,[1,2] and the promise of higher-precision measurements,[3] observation of weak radiative corrections or the nuclear "anapole" moment[4] have become enticing possibilities. To distinguish these contributions from the "normal" parity-violating amplitude requires that the atomic calculations be accurate to within a few percent.[5,6] While some authors already claim to have achieved this precision,[7] general acceptance of this claim will occur only if the same theories are capable of predicting measured parity-conserving processes to the same precision. With the hope of providing such a test and as a prelude to our EDM measurement, we describe here precision measurements of the Stark shifts associated with the cesium D lines.

II. THEORY

In the presence of an external electric field ε, the shifts of the various magnetic sublevels of a particular electronic state may be expressed in terms of scalar and tensor polarizabilities, α_0 and α_2. If the atomic hyperfine structure is neglected, the energy shift of a particular magnetic sublevel may be expressed in terms of its total angular momentum J and its projection along the quantization axis z,[8]

$$W(J,m_J)=-\tfrac{1}{2}\alpha_0\varepsilon^2-\tfrac{1}{2}\alpha_2\frac{3m_J^2-J(J+1)}{J(2J-1)}\left[\frac{3\varepsilon_z^2-\varepsilon^2}{2}\right],$$

where

$$\alpha_0=-\tfrac{2}{3}\sum_{J'}\frac{|\langle J\,|\,p\,|\,J'\rangle|^2}{(2J+1)[E(J)-E(J')]} \tag{1}$$

and

$$\alpha_2=2\left[\frac{10J(2J-1)}{3(2J+3)(J+1)(2J+1)}\right]^{1/2}\times\sum_{J'}\frac{|\langle J\,|\,p\,|\,J'\rangle|^2}{E(J)-E(J')}(-1)^{J+J'+1}\begin{Bmatrix}J & J' & 1\\ 1 & 2 & J\end{Bmatrix}.$$

Here $E(J)$ is the energy of the state J and the summation over J' includes all the atomic levels for which the matrix elements of the dipole-moment operator p are nonzero. These matrix elements in the J basis may be expressed in the L basis as

$$|\langle J\,|\,p\,|\,J'\rangle|^2=(2J+1)(2J'+1)\begin{Bmatrix}L & J & S\\ J' & L' & 1\end{Bmatrix}^2\times|\langle L\,|\,p\,|\,L'\rangle|^2.$$

For a single-electron atom the elements may be written as

$$|\langle L\,|\,p\,|\,L'\rangle|^2=e^2l_>\left[\int_0^\infty R_n r R_{n'}dr\right]^2,$$

where $l_>$ is the greater of l and l'.

If the hyperfine structure is not negligible then the above analysis must be extended to include the nuclear spin I. If we assume that the Stark shift is small compared to the hyperfine splitting, each magnetic sublevel m_F of a hyperfine level F is shifted by an energy[9]

$$W(F,m_F)=-\tfrac{1}{2}\alpha_0\varepsilon^2-\alpha_2\frac{[3m_F^2-F(F+1)][3X(X-1)-4F(F+1)J(J+1)]}{(2F+3)(2F+2)2F(2F-1)2J(2J-1)}(3\varepsilon_z^2-\varepsilon^2), \tag{2}$$

where $X=F(F+1)+J(J+1)-I(I+1)$.

Because $J=\frac{1}{2}$ for the $6S_{1/2}$ and $6P_{1/2}$ levels there is no tensor shift associated with these states. In higher order the hyperfine components of these levels acquire some tensor polarizability;[10] however, at the sensitivity of the present experiment these terms are completely negligible. The anticipated scalar polarizabilities for these levels may be deduced from Eq. (1),

$$\alpha_0(S_{1/2})=\tfrac{1}{9}[C(s,p_{1/2})+2C(s,p_{3/2})]$$

and

$$\alpha_0(P_{1/2})=\tfrac{1}{9}[C(p_{1/2},s)+2C(p_{1/2},d_{3/2})]\ ,$$

where

$$C(l,l')=2e^2\sum_{n'}\frac{\left[\int_0^\infty R(nl)R(n'l')r\,dr\right]^2}{E(nl)-E(n'l')}\ .$$

Similarly, for the $P_{3/2}$ level the scalar and tensor polarizabilities may be expressed as

$$\alpha_0(P_{3/2})=-\tfrac{1}{45}[9C(p_{3/2},d_{5/2})+C(p_{3/2},d_{3/2})+5C(p_{3/2},s)]$$

and

$$\alpha_2(P_{3/2})=\tfrac{1}{225}[9C(p_{3/2},d_{5/2})-4C(p_{3/2},d_{3/2})+25C(p_{3/2},s)]\ .$$

The results derived here agree with the expressions that may be derived from Ref. 11.

III. PRINCIPLE OF THE EXPERIMENT

The basic principle of the experiment is to observe the shift of the peak of the cesium absorption profile when an external electric field is applied. The absorption is monitored by illuminating the Cs vapor with a single-mode laser tuned to a particular resonance line and monitoring the transmission with a photodiode. The laser frequency is modulated sinusoidally at a frequency f. Lock-in detection of the transmission at this frequency yields a signal that is proportional to the slope of the absorption profile at the center frequency of the modulation (Fig. 1). At the peak of the absorption profile this derivative signal passes through zero. The shift of this zero-derivative frequency when an external electric field is applied is then observed.

IV. THE APPARATUS

A schematic of the apparatus used is shown in Fig. 2. The experimental cells are fabricated from 1 in.$\times$1 in. Pyrex tubing with two 1.5 in.$\times$1.5 in. electrodes attached with Torr-Seal epoxy to form the top and bottom of the cell. Typically the electrodes are spaced one centimeter apart; however, one cell was fabricated with a spacing of 4 mm. A variety of electrode materials has now been used including solid tantallum, molybdenum, zirconium, and stainless steel, as well as glass coated with either titanium nitride or platinum. With the exception of molybdenum, all of the materials are found to be acceptable. Due to difficulties associated with differential expansion, however, the coated-glass electrodes are preferable.

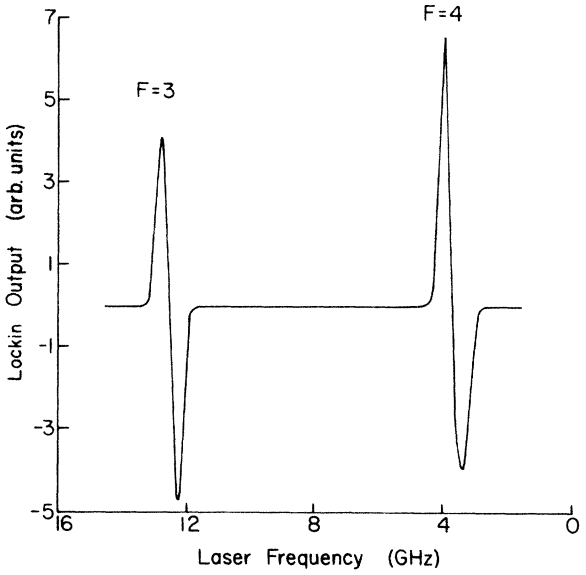

FIG. 1. Absorption scan across the $6S_{1/2}$-$6P_{3/2}$ transition at 8521 Å. The laser frequency is modulated at a frequency $f\approx 1$ kHz as it is scanned. The curve shown is the output of a lock-in detector monitoring the modulation of the transmission at f. The hyperfine splitting of the ground state is clearly resolved. The unresolved $6P_{3/2}$ hyperfine structure is responsible for the asymmetry in the curves.

The cesium is introduced into the cells by vacuum distillation. It is found that to achieve comparable vapor pressures, substantially more cesium must be distilled into a cell with electrodes than into a similar cell fabricated entirely from glass. The cesium appears to migrate into the metal surfaces, liberating some gas in the process (probably hydrogen). A siliconizing agent (Surfa-Sil) has been used to coat the inner surfaces of some of the cells.

The measurements have been performed with two different laser systems. Single-mode laser diodes that operate at 8944 and 8521 Å (Mitsubishi ML-2701) have been procured. With temperature stabilization to 0.1 m°C and good current regulation, passive center-frequency stability of about 10 MHz over a few minutes of operation has been achieved. Fine tuning of the laser diode frequency is accomplished by varying the diode injection current. By controlling this current with the derivative absorption signal from a cesium cell, the diode laser can be locked to the center of an absorption line. In this manner the center-frequency jitter of the laser diode is reduced to about 100 kHz.

The second laser system used is a ring dye laser (Coherent CR-699-21) pumped by an 8-W all-lines argon-ion laser. The laser is operated with Styryl-9M laser dye. Excellent performance of this system has been observed at 8521 Å. Due to the extremely low gain of the dye at 8944 Å, operation at this wavelength has been difficult and generally short lived. The ring dye laser is stabilized with an external etalon assembly. Drifts in this

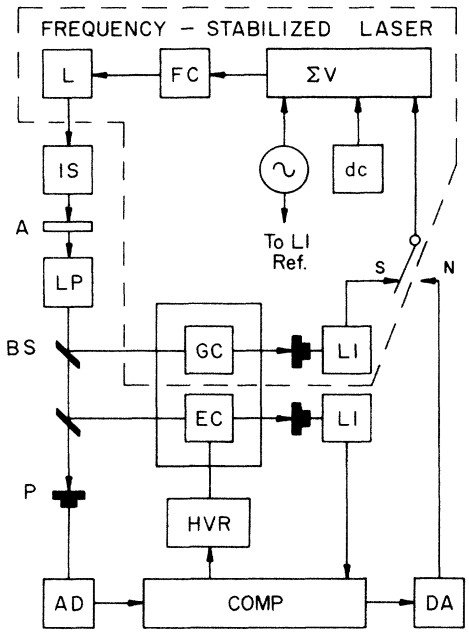

(a)

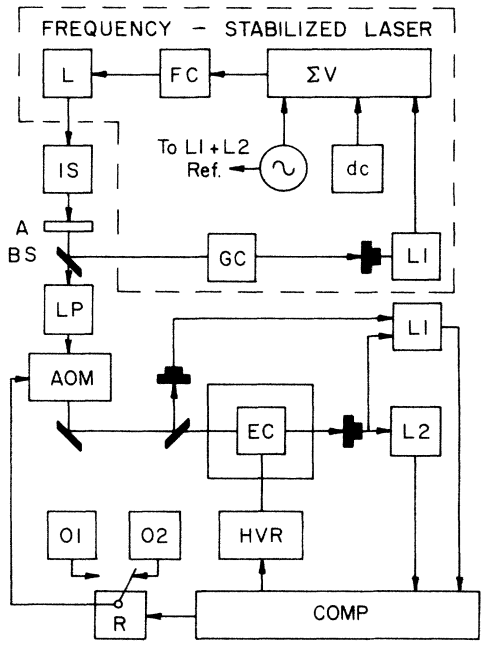

(b)

FIG. 2. Schematic of the apparatus used in (a) method 1 and (b) method 2: L, laser; IS, intensity stabilizer; A, optical attenuator; LP, linear polarizer; BS, beam splitter; P, photodiode; GC, glass cell; EC, cell with electrodes; AD, analog-to-digital converter; HVR, high voltage relay; COMP, computer; DA, digital-to-analog converter; LI, lock in (frequency f); L2, lock in (frequency $2f$); S/N, switch position for "Stark" or "normalization" data; ΣV, voltage sum; FC, laser frequency control; AOM, acousto-optic modulator; R, relay; 01 and 02, radio-frequency oscillators.

system of a few MHz over a five-minute period are typical. Using a scheme similar to that described for the diode laser, the ring may also be locked onto an atomic resonance line. This results in a reduction of the ring laser's center-frequency jitter to a few hundred kHz.

Light detection is accomplished using 1-cm^2 photodiodes (Hamamatsu S-1723). The dc currents from the photodiodes are measured with electrometers (Keithley 610-C) while the various modulated signals are monitored with lock-in detectors (Stanford Research SR-510). The resulting signals are digitized and stored (a D.E.C. Minc-23 data-acquisition system was used in our first measurements, an IBM PC AT was used in later work). The computer controls high-voltage relays that turn the applied Stark field on and off or reverse its polarity.

V. EXPERIMENTAL METHOD

Two different methods of frequency calibration have been used. In the first method the laser is tuned between the transitions originating from the $F=3$ or $F=4$ hyperfine levels of the ground state by applying an external dc voltage to the laser-frequency controller. With the known splitting between the various hyperfine components, the calibration between the externally applied voltage and the change in laser frequency can be determined. Care must be taken when calibrating the transitions to $6P_{3/2}$ due to the unresolved hyperfine structure of the excited state. With the inclusion of the upper-state hyperfine structure, the expected separation between the experimental zero crossings for transitions originating in the $F=3$ and $F=4$ hyperfine components of the ground state is 8.77 GHz, not the 9.19 GHz ground-state hfs splitting. While the incident laser is locked to the absorption line center in a field-free cell, the change in the lock-in signal from a second cell is recorded when an external electric field is applied and then removed. This procedure is repeated many times for both field polarities, and the data are analyzed in a manner that eliminates any systematics associated with uniform drifts in the laser frequency. The laser is then unlocked from the atomic line and the voltage required to tune the laser to produce an equivalent change in the lock-in signal is similarly determined. With the previously measured calibration of the laser's frequency-to-voltage characteristics a value of the Stark shift may be deduced. While straightforward, this method suffers from two principal limitations. First, the laser must be unlocked from the atomic resonance in order to calibrate the Stark-shift measurement. This results in unnecessary noise associated with drifting of the laser frequency. This is especially a problem for the diode lasers where locking to the atomic resonance is the only active method of frequency stabilization. The second limitation of the method is that one must assume a linear response of the laser-tuning circuitry between a few MHz and 9 GHz. While this assumption appears to be valid to the required precision for the diode lasers, it is clearly not true for the ring dye laser where a hysteresis effect of a few hundred kHz has been observed.

To overcome these difficulties a second method of cali-

bration was devised. The laser is continually locked onto a reference cell that has been pressure shifted by about 40 MHz through the introduction of about 6 torr of nitrogen gas. An acousto-optic modulator (Intra-Action Corp., AOM-40N) is then used to shift the laser frequency back 40 MHz so that it is on line center in the evacuated experimental cell. The laser frequency is, as usual, modulated at a frequency f. In addition to the lock-in detector monitoring transmission modulation at f, a second lock-in now detects the modulation at $2f$. This additional signal, proportional to the second derivative of the absorption curve, is nearly frequency independent over the range of typical Stark shifts and provides a background-free signal proportional to the transmitted laser intensity.

In order to observe the Stark shift an electric field is applied to the experimental cell. Simultaneously, the frequency of the AOM is shifted to a new frequency to approximately compensate for the induced Stark shift (typically 3–5 MHz). A plot of the change in the lock-in detector signal versus the difference of the frequencies applied to the AOM is shown in Fig. 3. The AOM frequency difference that yields no change in the lock-in output when the field is applied is easily deduced. This difference is effectively the Stark shift of the absorption maximum. A plot of the measured shift versus the square of the voltage is shown in Fig. 4.

While this new method of signal calibration overcomes both of the difficulties associated with the first method, it is subject to other possible systematic effects. In particular, the shifting of the AOM frequency also alters the position of the diffracted beam. Care must be taken in the optical design to ensure that differential clipping of the transmitted beam does not occur. This change in position of the beam with frequency can also result in changes in etalon effects in the various optical components. To reduce this effect to an insignificant level, the laser's intensity modulation is monitored just before the beam enters the cell. This signal is balanced with the transmitted beam and the two signals enter into the differential input of the lock-in detector. The resulting signal is free of the spurious intensity modulation.

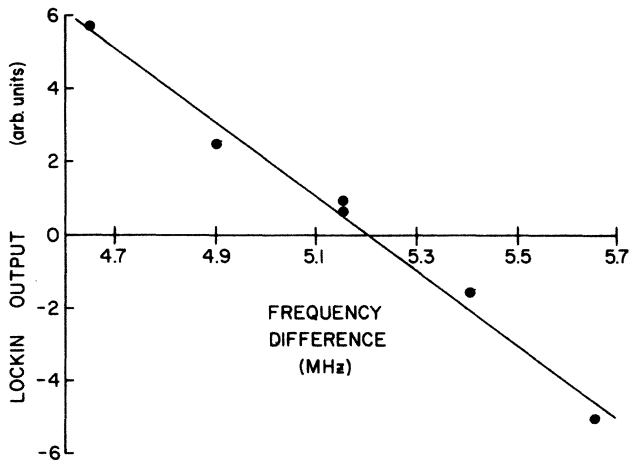

FIG. 3. Typical signal (method 2). The change in the lock-in output is plotted as a function of the difference between the radio frequency applied to the AOM with the electric field on (≈ 5 kV/cm) and off. The Stark shift of the absorption maximum is the frequency that yields no change in the lock-in output.

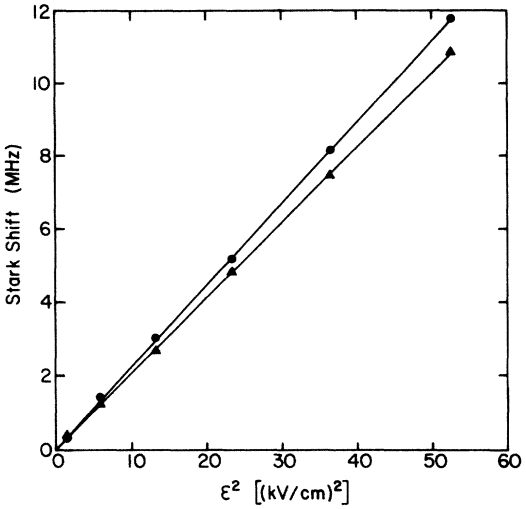

FIG. 4. Frequency shift of the absorption maxima as a function of the square of the applied electric field. The incident light is linearly polarized along the Stark field. The transition is from $6S_{1/2}$, $F=3$ (●) or $F=4$ (▲) to $6P_{3/2}$.

Contamination of the diffracted beam by the primary beam can result in a systematic overestimate of the Stark shift. Reduction of this systematic effect is accomplished with good spatial filtering. In addition, changes in the intensity of the diffracted beam with the change in the AOM frequency can result in different intensity-dependent shifts (either ac Stark shift or a shift due to partial saturation of the transition). This effect is reduced to an insignificant level by keeping the laser intensity low (~ 1 μW), the beam expanded (area, 0.5 cm^2) and the intensity difference of the diffracted beams less than 3%. In this manner the contributions from each of these possible systematic effects are maintained at less than a few tenths of one percent.

The calibration, reversibility, and homogeneity of the applied Stark field have been extensively studied. Despite the finite electrode size, if the voltage drops uniformly along the inner cell walls, the electric field within the cell will be uniform. This is easily demonstrated using the uniqueness theorem. Table I shows the relative size of the observed Stark shift as the laser traverses the cells at different locations for both polarities of the applied field. In cells not coated with Surfa-Sil, large nonreversing field inhomogeneities are observed. If the cell is inverted while maintaining a fixed orientation of the applied potential, the resulting pattern remains unchanged; this indicates that these inhomogeneities are not due to some geometrical imperfection in the cell. Observations on several uncoated cells all produce this same pattern. The field pattern indicates that the potential of the inner glass

TABLE I. The relative value of the observed Stark shift as a function of the position of the incident laser and the polarity of the applied voltage (HV + and HV −). The uncertainty in each measurement is between 0.01 and 0.02.

Vertical position from cell center (mm)	Horizontal position: Cell center HV +	Cell center HV −	Cell wall HV +	Cell wall HV −
	Uncoated cell			
4.5	0.68	1.43	0.51	1.60
3.0	0.79	1.26		
1.5	0.88	1.05		
0	0.99	1.01	0.93	1.08
−1.5	1.05	0.90	1.15	0.86
−3.0	1.24	0.84	1.36	0.71
	Surfa-Sil coated cell			
3.0	1.01	1.03		
1.5	0.99	1.01	0.99	1.02
0	1.01	1.00	0.98	0.99
−1.5	1.01	0.99	1.05	0.98
−3.0	1.02	1.01		

walls does not drop uniformly across the glass, but that it migrates preferentially toward the potential of the more positive electrode. This observation is not presently understood, but it seems to involve some sort of surface effect. The leakage currents across the cells are typically only a few hundred pA and are symmetric for the different polarities.

Also shown in Table I are similar measurements made on a cell whose inner surface has been coated with Surfa-Sil. Clearly the field homogeneity and reversibility are vastly better in this cell. Such uniform fields have only been observed in Surfa-Sil-coated cells. The leakage currents are not appreciably modified by the coating. Typically, after about six months of use, the field homogeneity of these cells also deteriorates, but the resulting inhomogeneities reverse when the cell is inverted, indicating that this effect is associated with a genuine electrical modification of the cells' dielectric surfaces.

The Stark measurements reported here are all performed in coated cells with good field homogeneity and reversibility. Four different cells are used, three with electrode spacings of about 1 cm and one with a spacing of about 4 mm. No significant difference in the measured Stark shift is observed between the different cells. In addition to the uncertainty associated with the field inhomogeneity, the uncertainties associated with the applied voltage (0.2%) and the cell spacing (0.2%) must also be taken into account.

VI. RESULTS

With the cells at 30 °C, an incident power of 1 μW, and a laser-frequency modulation amplitude of 80 MHz, the measured frequency shift of the absorption maxima are listed for the various transitions in Tables II and III. Application of an 8.5-G magnetic field does not significantly modify the results. The results are similarly insensitive to an increase in the Cs density by a factor of 4 or to an increase or decrease of the laser intensity by a factor of 5. At much higher laser intensities, significant changes are observed. These may be due to ac Stark effects, saturation, or optical pumping. A more detailed study of

TABLE II. $6S_{1/2}$-$6P_{1/2}$ Stark shift [kHz/(kV/cm)^2] of the various hfs transitions.

Transition (F-F')	Polarization with respect to ε	Method 1[a] ring laser	Method 2 ring laser	Method 2 diode laser	Average
3-4	∥	118±4	122±3	120.4±0.5	120.4±0.5
3-4	⊥		120±5	120.1±0.4	120.1±0.4
3-3	∥	116±4	123±4	120.6±1.3	120.4±1.2
3-3	⊥		113±3[b]	123.6±1.6	121.3±1.4
4-4	∥	119±4	122±4	121.9±0.5	121.5±0.5
4-4	⊥		118±3	120.6±0.7	120.5±0.7
4-3	∥	120±4	121±3	119.9±0.3	119.9±0.3
4-3	⊥		122±4	121.4±0.4	121.4±0.4
Average		118±4	119.7±1.2	120.6±0.2	120.6±0.2
Average (including all systematics)					120.6±1.2

[a]The 3% frequency-calibration uncertainty associated with the ring-laser measurements using method 1 is included.

[b]This is chronologically the last measurement taken at 8944 Å with the ring laser. The laser intensity fell rapidly and the intensity stabilization circuity was unable to maintain a constant intensity. Because of a failure in our argon-ion tube, we were unable to repeat this measurement. The data are included for completeness; however, because of the adverse conditions the deviation from the mean of the other data should not be regarded as significant. The inclusion or rejection of this point does not significantly alter the final average.

TABLE III. $6S_{1/2}$-$6P_{3/2}$ Stark shift [kHz/(kV/cm)^2] for transitions originating in a specific ground-state hfs level. The upper-state hfs is unresolved. Systematic effects in the uncertainties have been included throughout the table.

Initial state	Polarization with respect to ε	Method 1 diode laser	Method 2 ring laser	Method 2 diode laser	average
$F=3$	$\parallel$	211±2	214±2	212±2	212±2
$F=3$	$\perp$		131±2	128±2	130±2
$F=4$	$\parallel$	198±2	199±2	196±2	198±2
$F=4$	$\perp$		137±2	134±2	136±2

optical-pumping effects is presented in Appendix A.

Measurements on the $6S_{1/2}$-$6P_{1/2}$ transition are made on each of the four possible hyperfine transitions. The 1.168-GHz hyperfine splitting of $6P_{1/2}$ is easily resolved. As expected, there is no evidence for any tensor polarizability on the transitions from $6S_{1/2}$ to $6P_{1/2}$. The scalar shift is obtained by simply averaging the results for the various hyperfine components and light polarizations. The resulting scalar polarizability difference is shown in Table IV. These results may be combined with the measured value[15] of the $6S_{1/2}$ scalar polarizability, $\alpha_0(6S_{1/2}) = (59.6\pm1.2)\times10^{-24}$ cm^3, to yield values for the scalar polarizabilities of the P states.

Unlike the $J=\frac{1}{2}$ states, the $6P_{3/2}$ level has a significant tensor polarizability. The m-dependent part of the Stark Hamiltonian may be expressed as

$$\mathcal{H}=\frac{-3\alpha_2 J_z^2(3\varepsilon_z^2-\varepsilon^2)}{4J(2J-1)} .$$

The diagonal elements of this Hamiltonian are responsible for the m_F-dependent energy shift in Eq. (2). In addition, this Hamiltonian mixes the various $6P_{3/2}$ hyperfine levels,

$$|F',m_{F'}\rangle_{\rm mix} = |F',m_{F'}\rangle + \sum_{F''} \frac{\langle F'',m_{F'}|\mathcal{H}|F',m_{F'}\rangle}{E(F')-E(F'')} |F'',m_{F'}\rangle .$$

This mixing results in a modification of the excitation probability to the various hyperfine components involved in the transition from the ground state,

$$P(F',m_{F'}) = |\langle F,m_F|E_1|F',m_{F'}\rangle_{\rm mix}|^2 \approx |\langle F,m_F|E_1|F',m_{F'}\rangle|^2 + 2\,{\rm Re}\sum_{F''} \frac{\langle F,m_F|E_1|F'',m_{F'}\rangle\langle F'',m_{F'}|\mathcal{H}|F',m_{F'}\rangle\langle F,m_F|E_1|F',m_{F'}\rangle^*}{E(F')-E(F'')}$$

Here E_1 represents the electric dipole transition operator and terms of second order in the Stark-shift energy divided by the hyperfine splitting are neglected. The validity of this approximation for the electric fields used is well established by the experimental results.

With the linear polarization of the excitation radiation assumed to be along $\hat{\mathbf{z}}$, only matrix elements with $m_F=m_{F'}$ will be nonzero. The calculated relative excitation probabilities to each of the magnetic sublevels of each hyperfine component in the presence of the external field are listed in Table V. Because the hyperfine structure of the $6P_{3/2}$ level is unresolved in our experiment, this modification of the relative excitation probabilities results in a shift in the total absorption profiles maxima and must be taken into account in interpreting our experimental results. Indeed, neglecting these rate modifications leads to an overestimate of the atomic tensor polarizability by more than a factor of 3.

To deduce the scalar shift of the $6P_{3/2}$ transition, the tensor contribution must be eliminated. From Eq. (2) and Table IV it is evident that the tensor contribution to the shift may be removed by summing the shift observed

TABLE IV. Cs polarizabilities (10^{-24} cm^3).

Polarizability	Theory Ref. 12	Theory Ref. 13	Theory Ref. 14	Experiment Ref. 11	Experiment Present results
$\alpha_0(P_{1/2})-\alpha_0(S_{1/2})$	136	122	117	135±28	143.8±1.4
$\alpha_0(P_{3/2})-\alpha_0(S_{1/2})$	163	172	169	182±25	187.3±1.9
$\alpha_2(P_{3/2})$	−28	−37	−37	−39±25	−38.5±1.2

TABLE V. The relative absorption probabilities of the various magnetic sublevels for transitions from $6S_{1/2},F,m_F$ to $6P_{3/2},F',m_{F'}$. The light is assumed to be linearly polarized along z, leading to the selection rule $m_F=m_{F'}$. The parameters χ and Δ_{mn} are defined as $\chi\equiv(-\alpha_2/4)(3\varepsilon_z^2-\varepsilon^2)$ and $\Delta_{mn}\equiv E_m-E_n$.

F	F'	Relative transition probability
4	3	$[(16-m_F^2)/432]\left[1-\frac{m_F^2}{5}\frac{\chi}{\Delta_{43}}+\frac{2}{15}(25-m_F^2)\frac{\chi}{\Delta_{53}}\right]$
4	4	$[7m_F^2/720]\left[1+\frac{2}{15}(25-m_F^2)\frac{\chi}{\Delta_{54}}+\frac{(16-m_F^2)}{21}\frac{\chi}{\Delta_{43}}\right]$
4	5	$[(25-m_F^2)/135]\left[1-\frac{7m_F^2}{40}\frac{\chi}{\Delta_{54}}-\frac{(16-m_F^2)}{24}\frac{\chi}{\Delta_{53}}\right]$
3	2	$[(9-m_F^2)/63]\left[1+\frac{3m_F^2}{8}\frac{\chi}{\Delta_{32}}+\frac{5}{16}(16-m_F^2)\frac{\chi}{\Delta_{42}}\right]$
3	3	$[m_F^2/48]\left[1-\frac{2(9-m_F^2)}{7}\frac{\chi}{\Delta_{32}}+\frac{(16-m_F^2)}{21}\frac{\chi}{\Delta_{43}}\right]$
3	4	$[5(16-m_F^2)/1008]\left[1-\frac{2}{7}(9-m_F^2)\frac{\chi}{\Delta_{42}}-\frac{m_F^2}{5}\frac{\chi}{\Delta_{43}}\right]$

when the electric field is parallel to the linear-polarization axis with twice the shift observed when the electric field is perpendicular to $\hat{\mathbf{z}}$ and dividing by 3. This is equivalent to noting that if one begins with equal occupation probabilities of the various magnetic sublevels of the ground state and excites with equal intensities of light linearly polarized along $\hat{\mathbf{x}}$, $\hat{\mathbf{y}}$, and $\hat{\mathbf{z}}$, then the resulting population of the excited state must be distributed equally among the various magnetic sublevels of each hyperfine level. In addition, the relative probability of excitation to each hyperfine level will be the same as in zero field. The shift associated with this spherically symmetric excitation is the scalar shift. The scalar shift associated with the transitions originating in either the $F=3$ or $F=4$ hfs components of the ground state thus deduced from Table III are, respectively, 157.3 ± 1.5 kHz/(kV/cm)^2 and 156.7 ± 1.5 kHz/(kV/cm)^2. The agreement between these independent results is good. The resulting scalar polarizability difference is shown in Table IV. We note that the same results are obtained if the computer model that will now be described is instead used to extract the scalar shift.

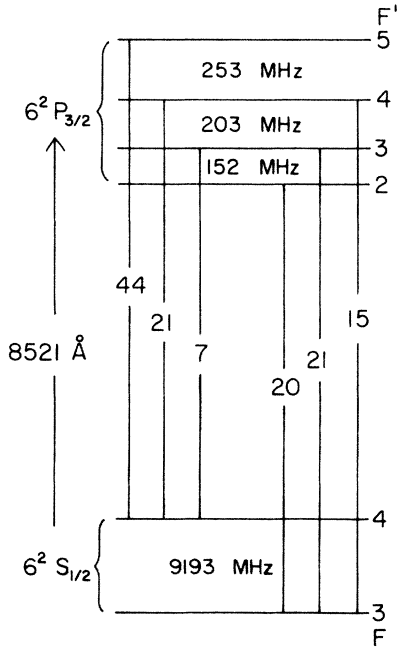

FIG. 5. The $6S_{1/2}$-$6P_{3/2}$ energy levels and relative transition probabilities with zero electric field.

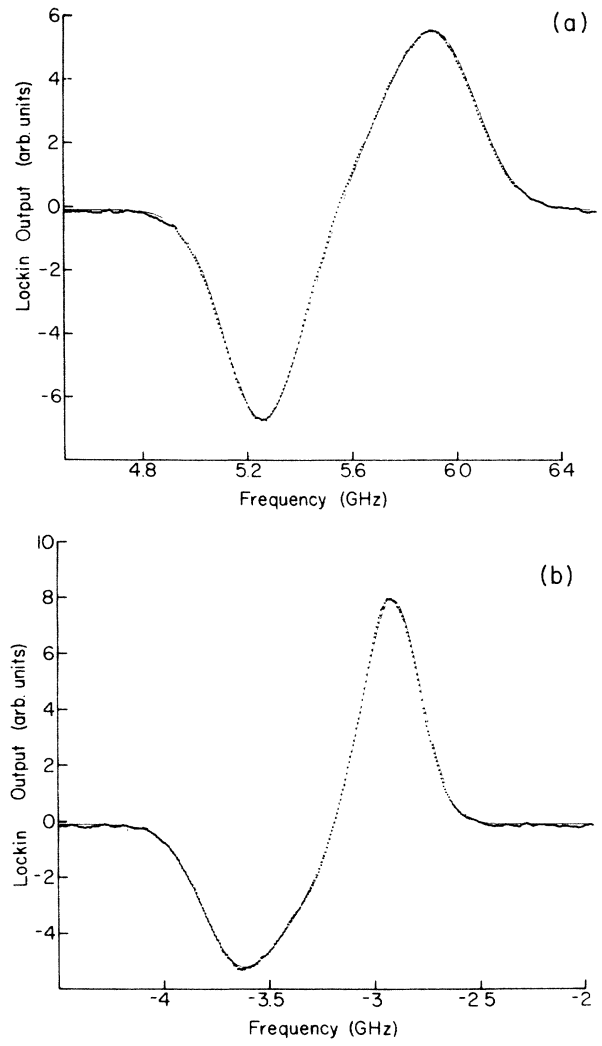

FIG. 6. Theoretical fit (solid line) of the lock-in signal (dots) vs laser frequency for the $6S_{1/2}$-$6P_{3/2}$ transition. (a) and (b) are, respectively, the transitions originating in the $F=3$ and $F=4$ hyperfine levels of $6S_{1/2}$. Both transitions are fit using a single amplitude, Gaussian width, and absorption length. The best-fit Gaussian width has a full width at half maximum of 410 MHz, in good agreement with the anticipated convolution of the 400-MHz line profile with the 6-MHz frequency modulation amplitude. No electric field is applied during these scans.

The tensor polarizability of the $6P_{3/2}$ state is somewhat more difficult to extract from the data because the observed shifts are a composite of the different shifts of the various magnetic sublevels of the unresolved hyperfine-structure components of the excited state. A computer model of the experimental signal is required in order to infer the tensor polarizability. The anticipated absorption profile from each ground-state hfs component can be calculated assuming a Gaussian profile (see Appendix B) for each of the various sublevels with the appropriate relative transition amplitude taken from Table V and with the hfs levels separated by the intervals shown in Fig. 5. In the limit of small modulation amplitude of the laser frequency, the output of the lock-in detector (monitoring at frequency f) is proportional to the derivative with respect to frequency of the experimental absorption curve. In Fig. 6 the lock-in output versus laser frequency is shown fit to the derivative of the anticipated absorption signal. The adequacy of the model is well demonstrated by the good agreement between the observed and theoretical line shapes.

For a given value of the atomic polarizability and a specific orientation of the illuminating polarization with respect to the applied field, the above model can be used to predict the frequency shift of the "zero-slope" point when an electric field is applied. The values of the tensor polarizability that yield our observed shifts for transitions originating in $F=3$ and $F=4$ are listed in column 1 of Table VI.

A further refinement of the model includes the effects of the finite modulation amplitude of the lock-in signal. To do this, we simulate the lock-in detector's response by sinusoidally modulating the frequency of the incident light and Fourier analyzing the resulting modulation in the calculated transmission through a cesium cell. The frequency at which the lock-in output is expected to be zero is thus numerically determined both for field off and for field on with various values of the tensor polarizability. The values of α_2 that yield the experimentally observed shifts with the application of the applied field are summarized in Table VI. The agreement between the deduced polarizabilities from the transition originating in the $F=3$ and $F=4$ hfs sublevels is quite good. The deduced tensor polarizability, including experimental and model-dependent uncertainties, is shown in Table IV.

VII. DISCUSSION

There is good agreement between our results for the scalar and tensor polarizabilities and those obtained by previous experiment and theory. Our results represent over an order of magnitude improvement in the precision of these measurements and should provide a good test of various new atomic theories. Stark-induced hyperfine mixing has been found to play an important role in the dipole transition rates to the various hyperfine components of the $6P_{3/2}$ state. This effect will have to be carefully considered as a potential source of systematic errors in experiments that search for atomic electric dipole moments using transitions to states with J greater than one half.

ACKNOWLEDGMENTS

We wish to acknowledge the excellent technical support provided by Donald Martin, William Slocombe, and Phillip Grant. We are indebted to Professor Norvel Fortson and Dr. Marie Anne Bouchiat and their groups for technical assistance and Professor Robert Hallock and Professor Stuart Crampton for important equipment loans. We thank James Watson and Peter Sheldon for computational assistance and Professor Robert Hilborn for useful conversations. This research was supported by grants from The National Science Foundation Research at Undergraduate Institutions Program, the National Bureau of Standards Precision Measurement Program, the William and Flora Hewlett Foundation of Research Corporation, and Amherst College. One of us (L.R.H.) would also like to acknowledge the generous support of the A.P. Sloan Foundation.

TABLE VI. The value of $\alpha_2(6P_{3/2})$ in units of 10^{-24} cm^3 deduced from various models of the experimental signal. The input parameters are the observed shifts, the hyperfine intervals, the effective Gaussian linewidth, Eq. (2), and Table V.

Initial hyperfine component F	Model of the experimental signal					
	1[a]	2[b]	3[c]	4[d]	5[e]	6[f]
$F=3$	−38.5	−39.1	−39.1	−38.5	−39.7	−38.5
$F=4$	−39.2	−38.3	−38.3	−39.2	−37.7	−38.9

[a]The Gaussian profiles (FWHM=390 MHz) from each of the magnetic sublevels are summed numerically and the shift in the composite profiles maximum when the Stark field is applied is fit to the experimental observations.

[b]The composite line profile is determined as in footnote a. The effects of the finite (80 MHz) frequency modulation amplitude are included as described in the text. One absorption length is assumed. This is the best approximation of the experimental situation.

[c]The same as footnote b except that two absorption lengths are assumed.

[d]The same as footnote b except that a 10-MHz frequency modulation amplitude is assumed. As expected, this result approaches the results of the method used in footnote a.

[e]The same as footnote b except that the effective Gaussian width (FWHM) is assumed to be 400 MHz.

[f]The same as footnote b except that the effective Gaussian width (FWHM) is assumed to be 380 MHz.

APPENDIX A

The measurements described here are performed with linearly polarized light that can create an alignment of the cesium ground state by optical pumping. For $6S_{1/2}$-$6P_{3/2}$, transitions from the different magnetic sublevels experience different Stark shifts due to the tensor polarizability of the $6P_{3/2}$ level. Significant alignment of the Cs ground state could thus result in a change in the observed Stark shift. In particular, this effect would result in an erroneous value of α_2. Because the observed shift is insensitive to either an increase or decrease in the laser intensity by a factor of 5, such a process is ruled out. However, in order to further investigate this possible systematic effect we have studied the optical pumping of the cesium ground state in our experimental cells. The cesium was pumped with 8521-Å radiation, propagating along $\hat{\mathbf{x}}$ and linearly polarized along $\hat{\mathbf{z}}$. The absorption of a weak 8944-Å probe beam (~ 1 μW) propagating along $\hat{\mathbf{y}}$ was monitored with our usual detectors. The linear polarization of the probe beam was modulated between $\hat{\mathbf{x}}$ and $\hat{\mathbf{z}}$ at 100 kHz by a photoelastic modulator (Hinds International). Lock-in detection at 100 kHz results in a signal that is proportional to the alignment of the cesium ground state. The resulting lock-in signal is shown in Fig. 7. In this figure the pump radiation is tuned to the transitions from $6S_{1/2}$, $F=4$ to $6P_{3/2}$, while the probe is tuned to the $6S_{1/2}$, $F=4$ to $6P_{1/2}$, $F=4$ transition. This configuration of pump and probe tuning was found to produce the largest polarization signals. Also shown in Fig. 7 is a fit to a saturation curve $S=S_\infty I/(I+I_0)$, where I is the pump-laser power, S_∞ is the lock-in signal at infinite power, and I_0 is the intensity that produces $\frac{1}{2}$ the maximum power. Assuming that the maximum alignment is unity, one finds that the ground state alignment for a pump power of 1 μW is approximately 6×10^{-5} and hence is completely negligible for our experiment.

Theoretically, the small polarization of the Cs ground state is due to the rapid depolarization rate ($\sim 2\times 10^4$ sec^{-1}) associated with the collisions of the Cs atoms with the metal electrodes. By contrast, the alignment pump rate is only about 1 sec^{-1} at 1 μW.

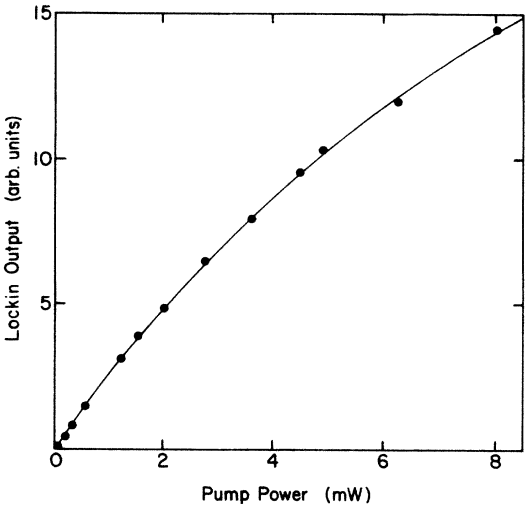

FIG. 7. Alignment of the cesium ground state as a function of pump-laser power. The experimental data (dots) are fit to a saturation curve (solid line).

APPENDIX B

The anticipated absorption profile is, of course, a Voigt profile and not a Gaussian. At the temperature of operation (30 °C) the Doppler profile has a full width at half maximum (FWHM) of 381 MHz. Natural broadening yields a Lorentzian with a FWHM of 4.8 MHz. For the ring laser the laser linewidth is negligible. We find that the linewidth of the diode laser must be approximately 30 MHz (FWHM) in order to understand Fig. 6. A Voigt convolution of a 381-MHz Gaussian and a 30-MHz Lorentzian has been fit to a Gaussian profile. The best-fit Gaussian has a FWHM of 400 MHz and does not deviate from the exact Voigt profile by more than 0.4% of the peak over the region within 500 MHz of line center. By contrast, a 10-MHz error in the Gaussian linewidth results in deviations over this same region of 2% of the peak. The effect of this more drastic change in the line profile is considered in Table VI. We conclude that the broadened Gaussian profile is quite adequate for modeling the experimental lines. Since the results for the ring and diode lasers are approximately equally weighted in our analysis of the $6P_{3/2}$ tensor polarizability, an effective Gaussian profile with a FWHM of 390±10 MHz is assumed.

[1]M. A. Bouchiat, J. Guena, L. Hunter, and L. Pottier, Phys. Lett. B **117**, 358 (1982); **134**, 463 (1984); J. Phys. (Paris) **47**, 1709 (1986); M. A. Bouchiat, J. Guena, and L. Pottier, *ibid.* **46**, 1879 (1985); **47**, 1175 (1986).

[2]S. L. Gilbert, M. C. Noecker, R. N. Watts, and C. E. Wieman, Phys. Rev. Lett. **55**, 2680 (1985); S. L. Gilbert and C. E. Wieman, Phys. Rev. A **34**, 792 (1986).

[3]M. A. Bouchiat and L. Pottier, Science **234**, 1203 (1986).

[4]V. V. Flambaum, I. B. Khriplovich, and O. P. Sushkov, Phys. Lett. B **146**, 367 (1984); Nucl. Phys. A **449**, 750 (1986); V. V. Flambaum (unpublished).

[5]W. R. Johnson, D. S. Guo, M. Idrees, and J. Sapirstein, Phys. Rev. A **32**, 2093 (1985); **34**, 1043 (1986).

[6]C. Bouchiat and C. A. Piketty, Europhys. Lett. **2**, 511 (1986).

[7]V. A. Dzuba *et al.*, Phys. Scr. (to be published); V. A. Dzuba, V. V. Flambaum, P. G. Silverstrov, and O. P. Sushkov, J. Phys. B **18**, 597 (1985).

[8]A. Khadjavi, A. Lurio, and W. Happer, Phys. Rev. **167**, 128 (1968).

[9]L. A. Armstrong, *Theory of Hyperfine Structure of Free Atoms* (Wiley, New York, 1971).

[10]J. R. P. Angel and P. G. H. Sandars, Proc. R. Soc. London,

Ser. A **305**, 125 (1968).
[11]R. Marrus, D. McColm, and J. Yellin, Phys. Rev. **147**, 55 (1966).
[12]D. R. Bates and A. Damgaard, Philos. Trans. R. Soc. London, Ser. A **242**, 101 (1949).
[13]P. M. Stone, Phys. Rev. **127**, 1151 (1962).
[14]M. Fabry, Can. J. Phys. **54**, 836 (1976).
[15]R. W. Molof, H. L. Schwartz, T. M. Miller, and B. Bederson, Phys. Rev. A **10**, 1131 (1974).